

AudioViewer: Learning to Visualize Sound

Yuchi Zhang
University of British Columbia
Vancouver, Canada
yuchi45@cs.ubc.ca

Willis Peng
University of British Columbia
Vancouver, Canada
williscpeng@gmail.com

Bastian Wandt
Leibniz University Hannover
Hannover, Germany
wandt@tnt.uni-hannover.de

Helge Rhodin
University of British Columbia
Vancouver, Canada
rhodin@cs.ubc.ca

Abstract

Sensory substitution can help persons with perceptual deficits. In this work, we attempt to visualize audio with video. Our long-term goal is to create sound perception for hearing impaired people, for instance, to facilitate feedback for training deaf speech. Different from existing models that translate between speech and text or text and images, we target an immediate and low-level translation that applies to generic environment sounds and human speech without delay. No canonical mapping is known for this artificial translation task. Our design is to translate from audio to video by compressing both into a common latent space with shared structure. Our core contribution is the development and evaluation of learned mappings that respect human perception limits and maximize user comfort by enforcing priors and combining strategies from unpaired image translation and disentanglement. We demonstrate qualitatively and quantitatively that our AudioViewer model maintains important audio features in the generated video and that generated videos of faces and numbers are well suited for visualizing high-dimensional audio features since they can easily be parsed by humans to match and distinguish between sounds, words, and speakers.

1. Introduction

Humans perceive their environment through diverse channels, including vision, hearing, touch, taste, and smell. Impairment in any of these modals of perception can lead to drastic consequences, such as challenges in learning and communication. Various approaches have been purposed to

substitute lost senses, going all the way to recently popularized attempts to directly interface with neurons in the brain (e.g., NeuraLink [39]).

One of the least intrusive approaches is to substitute audio and video, which is, however, challenging due to their high throughput and different modality. In this paper, we make a first step to visualize audio with natural images in real time, forming a live video that characterizes the entire audio content. It could be seen as an automated form of sign language translation, with its own throughput, abstraction, automation, and readability trade-offs. Figure 1 shows an example. Such a tool could help to perceive sound and also be used to train deaf speech, as immediate and high-throughput feedback on pronunciations is difficult to learn from traditional visual tools for the hearing-impaired speech learning that rely on spectrogram representations [12, 61, 60, 33].

Our long-term goal is to show that hearing-impaired persons can learn to perceive sound through the visual system. Similar to learning to understand sign language and likewise an unimpaired child learns to associate meaning to seen objects and perceived sounds and words, the user will have to learn a mapping from our sound visualization to its semantic. Still, articulation could be practiced by exploring the visual feedback space and speaking learned by articulating sounds that reproduce the same visual feedback as produced by the teacher or parent.

Translating an audio signal to video is difficult as there is no canonical one-to-one mapping across these domains with vastly different dimensions (one-dimensional audio to high-dimensional video) and characteristics (time-frequency representation to spatial structure). It is an open question of which visual abstraction level is best. Methods for digital dubbing and lip-syncing facial expressions from spoken

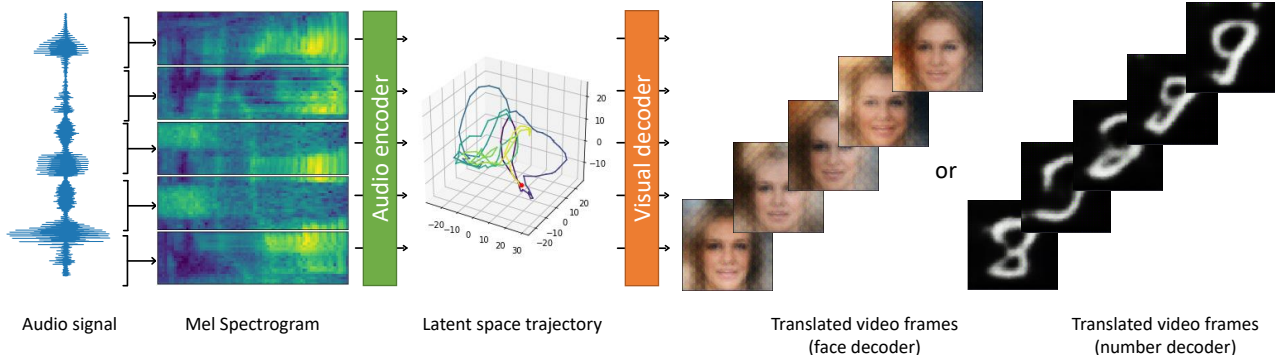


Figure 1. **AudioViewer**: A tool developed towards the long-term goal of helping hearing impaired persons to see what they can not hear. We map an audio stream to video and thereby use faces or numbers for visualizing the high-dimensional audio features intuitively. Different from the principle of lip reading, this can encode general sound and pass on information on the style of spoken language.

audio [10, 46, 59] would be natural, allowing deaf people to lip read. However, natural lip motion is rather a result of speaking and only contains a fraction of the audio information and does not apply to environment sounds. Another direction could be to translate speech to words with a recognition system [41], for example the spoken 'dog' would be translated to the text 'dog'. A conceivable extension is to further translate the word into an image using conditional generative adversarial networks (GANs) [16]. A dog image could be shown when the word 'dog' is recognized in the audio. This is intuitive, however, such a translation is still indirect and does not contain any vocal feedback or style differences between male and female speakers [49, 65, 42]. Moreover, events and ambient sounds that can not be indicated by a single word are ill-represented, such as the echo of a dropped object or the repeating beep of an alarm clock.

To overcome these limitations, we seek for an intuitive and immediate visual representation of the high-dimensional audio data and are inspired by early techniques from the 1970s that visualize general high-dimensional data with facial line drawings with varying length of the nose and curvature of the mouth [5, 25].

In this paper, we design an immediate audio to video mapping leveraging ideas from computer vision and audio processing for unpaired domain translation. The technical difficulty lies in finding a mapping that is expressive yet easy to perceive. We base AudioViewer on four principles. First, humans are good at recognizing patterns and objects that they see in their environment, particularly human faces [1, 28, 53, 5, 25]. We therefore map to videos that have the image statistics of natural images and faces. Second, humans are able to perceive complex spatial structure but quick and non-natural (e.g., flickering) temporal changes lead to disruption and tiredness [48]. Hence, we enforce smoothness constraints on the learned mapping. Third, frequent audio features should be mapped to frequent video features. We therefore exploit cycle consistency to learn a joint structure

between audio and video modalities. Fourth, we disentangle factors of variations, to separate style, such as gender and dialect, from content, individual phones and sounds.

Our core contributions are a new approach for enabling people to see what they can not hear; a method for mapping from audio to video via linked latent spaces; a quantitative analysis on the type of target videos, different latent space models, and the effect of smoothness constraints; and a first perceptual user study on the recognition capabilities. We demonstrate the feasibility of this AudioViewer approach with a working prototype and analyze the success by quantifying the loss of information content as well as showing that words and pronunciation can be distinguished from the generated video features in a user study.

2. Related Work

In the following section we first review the literature on audio and video generation, with a particular focus on cross-modal models. We then put our approach in context with existing assistive systems.

Classical audio to video mappings. Audio to video translation methods have mostly been designed for digital dubbing or lip-syncing facial expressions to spoken audio [10, 46, 59]. Other approaches reconstruct facial attributes, such as gender and ethnicity, from audio and generating matching facial images [58] and map music to facial or body animation [54, 29, 50, 47]. By contrast to our setting, all of these tasks can be supervised by learning from videos with audio lines, e.g., a talking person where the correspondence of lip motion, expressions and facial appearance to the spoken language is used to train the relation between sound and mouth opening. We go beyond spoken sounds and map to non-facial features such as background and brightness with an unsupervised translation mechanism.

Audio and video generation models. Image generation models predominantly rely on GAN [16] and VAE [32, 20]

formulations. The highest image fidelity is attained with hierarchical models that inject noise and latent codes at various network stages by changing their feature statistics [23, 30]. For audio, only few methods operate on the raw waveform [27]. It is more common use spectrograms and to apply convolutional models inspired by the ones used for image generation [21, 9, 2]. We use cross-modal VAE models as a basis to learn the important audio and image features.

Cross-modal latent variable models. CycleGAN and its variations [67, 51] have seen considerable success in performing cross-modal unsupervised domain transfer, for medical imaging [19, 56] and audio to visual translation [17], but often encode information as high frequency signal that is invisible to the human eye and susceptible to adversarial attacks [6]. An alternative approach involves training a VAE, subject to a cycle-consistency condition [26, 62], but these works were restricted to domain transfers within a single modality. Most similar is the joint audio and video model proposed by Tian et al. [55], which uses a VAE to map between two incompatible latent spaces using supervised alignment of attributes, however, it operates on a word not phoneme level, and has no mechanism to ensure temporal smoothness nor information throughput. Our contributions address these shortcomings. Relatedly, encoder-decoder and GAN models have been applied to generating video reconstructions of lip movements based on audio data [7, 4, 57, 66], however due to mapping ambiguities between phonemes and visemes, lip movements are not a reliable source of feedback for learning sound production [36, 40, 3, 13].

Deaf speech support tools. Improvements in speech production for the hearing impaired have been achieved through non-auditory aids and these improvements persist beyond learning sessions and extend to words not encountered during the sessions [49, 65, 42]. While electrophysiological [18, 31] and haptic learning aids [11] have demonstrated efficacy for improving speech production, such techniques can be more invasive, especially for young children, as compared to visual aids. Elssmann et al. [12] demonstrate visual feedback from the Speech Spectrographic Display (SSD) [49] is equally effective at improving speech production as compared with feedback from a speech-language pathologist. Alternative graphical plots generated from transformed spectral data have been explored by [61, 60, 33], which aim at improving upon spectrograms by creating plots which are more distinguishable with respect to speech parameters. Other methods aim at providing feedback by explicitly estimating vocal tract shapes [43]. In addition, Levis et al. [35] demonstrate that distinguishing between discourse-level intonation (intonation in conversation) and sentence-level intonation (intonation of sentences spoken in isolation) is possible

through speech visualization and argues that deaf speech learning could be further improved by incorporating the former. Commercially, products as such IBM’s Speech Viewer [24] are available to the public. Our image generation approach extends these spectrogram visualization techniques by leveraging the generative ability of VAEs in creating a mapping to a more intuitive and memorable video representation. It is our hope that improved visual aids will lead to more effective learning in the future.

Sensory substitution and audio visualization. Related to our work is the field of sensory substitution, whereby information from one modality is provided to an individual through a different modality. While many sensory substitution methods focus on substituting visual information into other senses like tactile or auditory stimulation to help visual rehabilitation [38, 22, 15], few methods target substituting auditory modal with visualization. Audio visualization is another field related to our work. Music visualization works generate visualizations of songs, so that user can browsing songs more efficiently without listen to them [63, 52]. On the learning side, [64] visualize the intonation and volume of each word in speech by the font size, so that user can learn narration strategies. Different from the works mentioned above, our model tries to visualize speech in phoneme level with deep learning models instead of hand-crafted features.

3. Method

Our goal is to translate a one-dimensional audio signal $\mathbf{A} = (\mathbf{a}_0, \dots, \mathbf{a}_{T_A})$ into a video visualization $\mathbf{V} = (\mathbf{I}_0, \dots, \mathbf{I}_{T_V})$, where $\mathbf{a}_i \in \mathbb{R}$ are sound wave samples recorded over T_A frames and \mathbf{I}_i are images representing the same content over T_V frames. Supervised training is not possible in the absence of paired labels. Instead, we utilize individual images and audio snippets without correspondence and learn a latent space \mathcal{Z} that captures the importance of image and audio features and translates between them with minimal information loss. Figure 2 shows the individual mapping steps. The audio encoder E_A yields latent code $\mathbf{z}_i \in \mathcal{Z}$ and the visual decoder $D_V(\mathbf{z}_i)$ outputs a corresponding image \mathbf{I}_i . This produces a video representation of the audio when applied sequentially. We start by learning individual audio and video models that are subsequently linked with a translation layer.

Matching sound and video representation. A first technical problem lies in the higher audio sampling frequency (16 kHz), that prevents a one-to-one mapping to 25 Hz video. We follow common practice and represent the one-dimensional sound wave with a perceptually motivated mel-scaled spectrogram, $\mathbf{M} = (\mathbf{m}_0, \dots, \mathbf{m}_{T_M})$, $\mathbf{m}_i \in \mathbb{R}^F$, where $F = 80$ is the number of filter banks. It is computed via the short-time Fourier transform with a 25ms Hanning window with 10 ms shifts. The resulting coefficients are converted to decibel

units flooring at -80dB. Because the typical mel spectrogram still has a higher sampling rate (100 Hz) than the video, we chunk it into overlapping segments of length $T_M = 20$ covering 200 ms. In the following, we explain how to map from mel segment to video frame.

3.1. Audio Encoding

Given unlabelled audio and video sequences, we start by learning independent encoder-decoder pairs (E_A, D_A) for sound and (E_V, D_V) for video. We use probabilistic VAEs since these do not only learn a compact representation of the latent structure, but also allow us to control the shape of the latent distribution to be a standard normal distribution. Let \mathbf{x} be a sample from the unlabelled audio set. We optimize over all samples the VAE objective [32]:

$$\mathcal{L}(\mathbf{x}) = -D_{\text{KL}}(q_\phi(\mathbf{z}|\mathbf{x})||p_\theta(\mathbf{z})) + \mathbb{E}_{q_\phi(\mathbf{z}|\mathbf{x})}(\log p_\theta(\mathbf{x}|\mathbf{z})), \quad (1)$$

with D_{KL} , the Kullback-Leibler divergence, and $q_\phi(\mathbf{z}|\mathbf{x})$ and $p_\theta(\mathbf{x}|\mathbf{z})$, the latent code and output domain posterior respectively. These have a parametric form, with

$$q_\phi(\mathbf{z}|\mathbf{x}) = \mathcal{N}(\boldsymbol{\rho}(\mathbf{x}), \boldsymbol{\omega}^2(\mathbf{x})\mathbf{I}) \quad \text{and} \quad (2)$$

$$p_\theta(\mathbf{x}|\mathbf{z}) = \mathcal{N}(\boldsymbol{\mu}(\mathbf{z}), \boldsymbol{\sigma}^2(\mathbf{z})\mathbf{I}), \quad (3)$$

where $\boldsymbol{\rho}$ and $\boldsymbol{\omega}$ the output of the encoder and $\boldsymbol{\mu}$ and $\boldsymbol{\sigma}$ the output of the decoder.

Audio network architecture. We use the SpeechVAE model from Hsu et al. [21] that is widely used for generative sound models. Fig. 2, left, sketches how the mel spectrogram is encoded with an encoder E_A of three convolutional layers followed by a fully connected layer which flattens the spatial dimensions. The mel spectrogram \mathbf{M} is a two-dimensional array, spanning the time and frequency, respectively. To account for the structural differences of the two, convolutions are split into separable $1 \times F$ and 3×1 filters, where F is the number of frequencies captured by \mathbf{M} and striding is applied only on the temporal axis. The decoder is symmetric to the encoder. We use ReLU activation and batch normalization layers in the encoder and decoder.

3.2. Structuring the Audio Encoding

We desire our latent space to change smoothly in time and disentangle the style, such as gender and dialect, from the content conveyed in phones.

Disentangling content and style. We construct a SpeechVAE that disentangles the style (speaker identity) content (phonemes) in the latent encodings, i.e., the latent encoding $\mathbf{z} = [z_1, \dots, z_d]^T \in \mathcal{R}^d$ can be separated as a style part $\mathbf{z}_s = [z_1, \dots, z_m]^T$ and a content part $\mathbf{z}_c =$

$[z_{m+1}, \dots, z_d]^T$, where d is the whole audio latent space dimension and m in the audio style latent space dimension.

To encourage such disentanglement we use an audio dataset with phone and speaker ID annotation. As it shows in Figure 3, at training time, we feed triplets of mel spectrogram segments $\{\mathbf{M}_{a,i}, \mathbf{M}_{b,i}, \mathbf{M}_{a,j}\}$, where $\mathbf{M}_{a,i}$ and $\mathbf{M}_{b,i}$ are the same phoneme sequence p_i spoken by different speakers s_a and s_b respectively, and $\mathbf{M}_{a,j}$ shares the speaker s_a with the first segment but a different phoneme sequence. Each element of the input triplet is encoded individually by E_A , forming latent triplet $\{\mathbf{z}_{a,i}, \mathbf{z}_{b,i}, \mathbf{z}_{a,j}\} = \{[\mathbf{z}_{s_a}, \mathbf{z}_{c_i}]^T, [\mathbf{z}_{s_b}, \mathbf{z}'_{c_i}]^T, [\mathbf{z}'_{s_a}, \mathbf{z}_{c_j}]^T\}$, instead of reconstructing the inputs from the corresponding latent encodings in an autoencoder, we reconstructed the first sample $\mathbf{M}_{a,i}$ from a recombined latent encoding of the other two, $\mathbf{z}'_{a,i} = [\mathbf{z}'_{s_a}, \mathbf{z}'_{c_i}]^T$. Formally, we replaced the reconstruction loss term in the VAE objective by a recombined reconstruction loss term,

$$\mathcal{L}_{rr}(\mathbf{T}_{a,b,i,j}) = \mathbb{E}_{q_\phi(\mathbf{z}'_{a,i}|\mathbf{M}_{b,i}, \mathbf{M}_{a,j})}(\log p_\theta(\mathbf{M}_{a,i}|\mathbf{z}'_{a,i})). \quad (4)$$

This setup forces the model to learn separate encodings for the style and phoneme information while not requiring additional loss terms.

Note that we could alternatively enforce $\mathbf{z}_{a,i}$ to be close to $\mathbf{z}'_{a,i}$ without decoding (the unused $\mathbf{z}_{a,i}$ in Figure 3). However, an additional L2 loss on the latent space led to a bias towards zero and lower reconstruction scores than the proposed mixing strategy that works with the original VAE objective.

Temporal smoothness. The audio encoder has a small temporal receptive field, encoding time segments of 200 ms. This lets encodings of subsequent sounds be encoded to distant latent codes leading to quick visual changes in the decoding. To counter act, we add an additional smoothness prior. We experiment with the following negative log likelihoods. For training the audio encoder, we sample a pair of input mel spectrogram segments $\{\mathbf{M}_i, \mathbf{M}_j\}$ at random time steps $\{t_i, t_j\}$, spaced at most 800ms apart, from the same utterance. We test the three different pair loss functions to enforce temporal smoothness in the embedded content vectors. First, by making changes in latent space proportional to changes in time,

$$\mathcal{L}_{p,MSE} = \frac{1}{N} \sum_i^N \left(\hat{\Delta}t_i - \|t_{i,1} - t_{i,2}\| \right)^2, \quad (5)$$

where the latent space dimension scale is learned by scalar parameter s , with $\hat{\Delta}t_i = s \cdot \|E_A(\mathbf{M}_i) - E_A(\mathbf{M}_j)\| = s \cdot \|\mathbf{z}_i - \mathbf{z}_j\|$ for models without style disentanglement, and $\hat{\Delta}t_i = s \cdot \|\mathbf{z}_{c,i} - \mathbf{z}_{c,j}\|$ for the disentangled ones, where the predicted time difference only calculated with the content part of the latent encodings. Second, we try whether

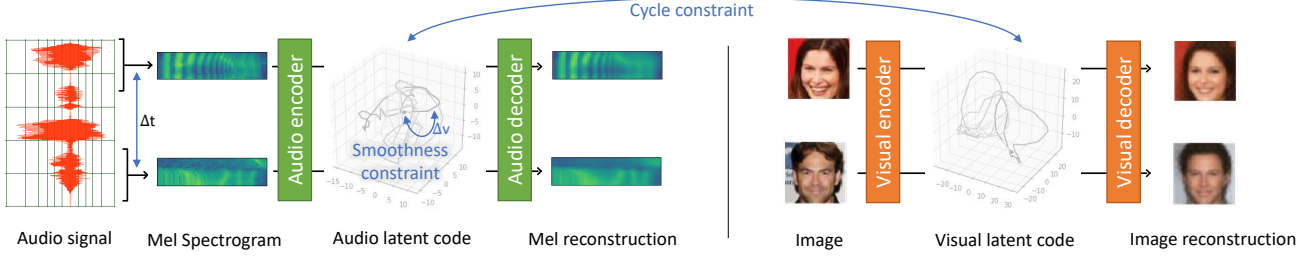


Figure 2. **Overview.** A joint latent encoding is learned with audio and video VAEs that are linked with a cycle constraint and augmented with a smoothness constraint (Δv annotation).

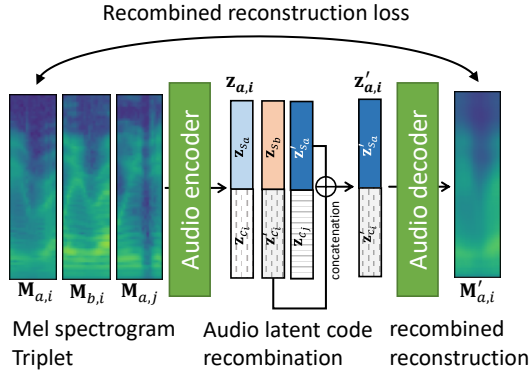


Figure 3. **Disentanglement,** by mixing content encodings from two speakers saying the same phones (\mathbf{z}_{c_i} with \mathbf{z}'_{c_i}) and style encodings from the same speaker saying different words (\mathbf{z}_{s_a} with \mathbf{z}'_{s_a}).

enforcing the ratio of velocities to be constant is better,

$$\mathcal{L}_{p,Q} = \frac{1}{N} \sum_i \left(\frac{\Delta \hat{t}_i}{\|t_{i,1} - t_{i,2}\|} - 1 \right)^2, \quad (6)$$

with learned scale as before. The same quotient constraint can also be measured in logarithmic scale,

$$\mathcal{L}_{p,\log MSE} = \frac{1}{N} \sum_i \left(\log \Delta \hat{t}_i - \log \|t_{i,1} - t_{i,2}\| \right)^2. \quad (7)$$

Our final model uses $\mathcal{L}_{p,\log MSE}$, which behaves better than quotients in our experiments. All objective terms are learned jointly, with weights $\lambda_{\text{cycle}} = 10$ and $\lambda_p = 10^3$ balancing their influence.

3.3. Image Encoding for Video Generation

Audio encoders and video decoders can be made compatible across modalities by using two VAEs with matching latent dimension and prior distribution $p(\mathbf{z})$ over $\mathbf{z} \in \mathcal{Z}$. We apply the per-frame image DFC-VAE model from Hou et al. [20]. The input image is passed through four 4x4 convolutional layers followed by a fully-connected layer to arrive at the latent code. The decoder uses four 3x3 convolutions.

Batch norm and LeakyReLU layers are applied between convolutions. Besides the per-pixel loss of the classical VAE, the DFC-VAE uses a perceptual loss in the feature space of a trained VGG-19 network for high-level feature consistency. This model is trained on individual videos but is applied sequentially to create the output video frames.

3.4. Linking Audio and Visual Spaces

By learning individual audio and video VAEs with the same latent space prior, we can concatenate the audio encoder with the image decoder for our desired AudioViewer translation. However, the learned encoders are only approximations to the true distribution and not all points in \mathcal{Z} are modelled equally well, leading to information loss. To bridge different latent space structures, we introduce an additional cycle constraint that works without image correspondence and ensures that samples from the audio latent space posterior are reconstructed well, similar in spirit to [26, 62]. Figure 4 shows the cyclic chaining from audio latent code to video and back. It is implemented on the content space as

$$\mathcal{L}_{\text{cycle}} = |E_V(D_V(\mathbf{z}_c)) - \mathbf{z}_c|, \quad (8)$$

where \mathbf{z}_c is drawn from the posterior of the content part $E_A(\mathbf{M})$ of the audio encoder and the video modules operate on mean values minimizing point-wise differences in position. Similar to the smoothness loss, the cycle loss can be applied to the disentangled models and visualize only the style part or content part as long as the latent dimension matches, so that the visualization can be content-agnostic or speaker-agnostic.

4. Experiments

In the following, we show qualitatively and quantitatively that AudioViewer conveys important audio features via visualizations of portraits or numbers and that it applies to speech and environment sounds. We provide additional qualitative results in the supplemental videos and document.

Quantitative metrics. We compare latent embeddings by the Euclidean distance, mel spectrogram with the signal to

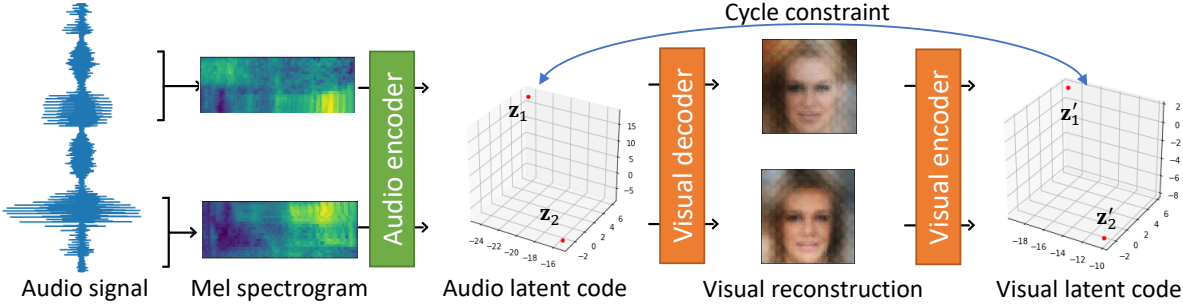


Figure 4. **Cycle constraint.** We link audio and video latent spaces with a cycle constraint that ensures that the audio signal content is preserved through video decoding and encoding.

noise ratio (SNR), Smoothness is measured as the change in latent space position.

Perceptual study. We perform a user study to analyze the human capability to perceive the translated audio content. Some results may be subjective and we therefore report statistics over 29 questions answered by 19 users. The study details are given in the supplemental document.

Baselines. We compare the proposed coupled audio-visual model and ablate using individual VAEs for audio and speech generation as well as when disabling the style-content disentangling. Furthermore, we ablate the latent space priors and training strategies introduced in section 3.2 and 3.4.

As a further baseline, we experiment with principal component analysis (PCA) for building a common latent space. PCA yields a projection matrix \mathbf{W} that rotates the training samples \mathbf{u}_i by $\mathbf{z}_i = \mathbf{W}\mathbf{u}_i$ to have diagonal covariance matrix Σ and maximal variance. We can use PCA for sound and images, with \mathbf{u} being either the flattened mel-segment $\text{vec}(M_i)$ or equivalently the flattened video frame $\text{vec}(I_j)$. We use the reduced PCA version, where \mathbf{W} maps to a Z_D dimensional space. We further scale rows of \mathbf{W} such that Σ is the identity matrix I . By this construction, the latent space has the same prior covariance as the VAE spaces. This encoding can be decoded with the pseudo-inverse \mathbf{W}^\dagger .

Audio Datasets. We use the TIMIT dataset [14] for learning speech embeddings. It contains 5.4 hours of audio recordings (16 bit, 16 kHz) as well as time-aligned orthographic, phonetic and word transcriptions for 630 speakers of eight major dialects of American English, each reading ten phonetically rich sentences. We use the training split (462/50/24 non-overlapping speakers) of the KALDI toolkit [45]. The phonetic annotation is only used at training time and as ground truth for the user study. In addition we report how well a model trained on speech generalizes to other sound on the ESC-50 dataset of environmental sounds [44] in the supplemental videos.

Image Datasets. To test what kind of visualization is best for humans to perceive the translated audio, we train and

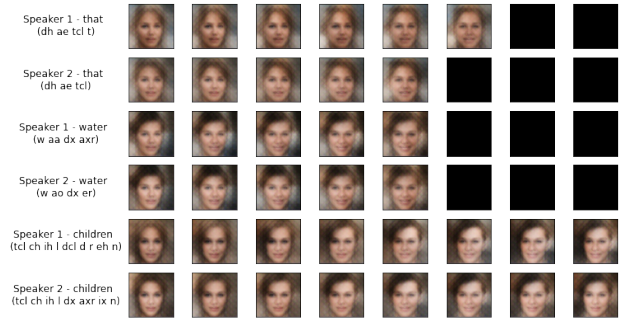


Figure 5. **Word analysis.** Instances (different rows) of the same words are encoded with a similar video sequence (single row), yet they show pronunciation variations if spoken by different speakers.

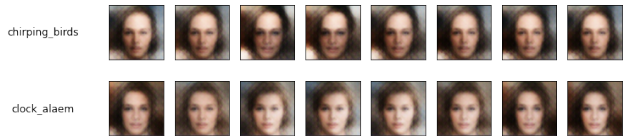


Figure 6. **Environment sounds visualization.** Although not trained for it, our approach also visualizes natural sounds. Here showing a clear difference between chirp and alarm clock.

test our model on two image datasets: The face attributes dataset CelebA [37] (162770/19962 images for train/val respectively), the MNIST [34] datasets (60000/10000 images for train/val respectively).

Training and runtime. Speech models are trained for 300 epochs with batch size 128 (65 pairs), CelebA models for 38 epochs and MNIST models for 24 epochs with batch size 144, and joint models are fine-tuned jointly on audio and image examples for 10 audio epochs. AudioViewer is real-time capable and we showcase a demonstration in the supplemental video, the amortized inference time for a frame is 5 ms on an i7-9700KF CPU @ 3.60GHz with a single NVIDIA GeForce RTX 2080 Ti.



Figure 7. **Phoneme similarity analysis.** The same phonemes occurring at the beginning of different words are mapped to visually similar images (columns) while different speakers have minimal influence (rows).

4.1. Visual Quality and Phonetics

A meaningful audio translation should encode similar sounds with similar visuals. Figure 7 depicts such similarity and dissimilarity on the first 200 ms of a spoken word since these can be visualized with a single video frame. This figure compares the content encoding to MNIST and faces, both are well suited to distinguish sounds. The same word (column) has high visual similarity across different speakers (F#: female, M#: male; # the speaker ID) and dialects (D#) while words starting with different sounds are visually different. Multiple frames of entire words are shown in Fig. 5. Our user study and supplemental document analyzes their differences in more detail and on entire sentences.

Although trained entirely on speech, our low-level formulation at the level of sounds enables AudioViewer to also visualize environment sounds. Figure 6 gives two examples.

4.2. Information Throughput

It is difficult to quantify the information throughput from audio to video as no ground truth is available and user studies are expensive. However, we can use the learned encoder and decoder to map from audio to video and back as a lower bound. This cyclic pattern lets us quantify the loss of information as the distance of the starting point to the reconstructed audio. Figure 8 gives an example and Table 1 summarizes relations quantitatively. The difference

Table 1. **Throughput lower bound.** The throughput from audio to video with AudioViewer can be bounded by mapping back to the audio. It is evident that the cycle consistency improves greatly while the enforcement of additional constraints with $\mathcal{L}_{p,\log MSE}$, and \mathcal{L}_{rr} , takes only a small dip.

Audio models	Visual models	SNR(dB)
Audio PCA	Visual PCA	23.37
SpeechVAE [21]	DFC-VAE on CelebA	1.65
	DFC-VAE on MNIST	2.01
	DFC-VAE on CelebA (refined w/ \mathcal{L}_{cycle})	4.43
	DFC-VAE on MNIST (refined w/ \mathcal{L}_{cycle})	0.78
SpeechVAE w/ $\mathcal{L}_{p,\log MSE}$, \mathcal{L}_{rr} , dim=256	DFC-VAE on CelebA	0.84
	DFC-VAE on MNIST	0.81
	DFC-VAE on CelebA (refined w/ \mathcal{L}_{cycle})	4.16
	DFC-VAE on MNIST (refined w/ \mathcal{L}_{cycle})	3.68

Table 2. **Audio encoding analysis.** The SNR of the autoencoder drops with the additional constraints we enforce (smoothness and disentanglement). This is a trade-off for improving velocity and acceleration properties as well as for inducing interpretability.

Audio models	SNR (dB)	Velocity (s^{-1})	Acc. (s^{-2})
Audio PCA	23.37	329.02	13395.11
SpeechVAE[21]	21.89	280.09	11648.17
SpeechVAE w/ $\mathcal{L}_{p,\log MSE}$	19.89	108.89	3052.19
SpeechVAE w/ \mathcal{L}_{rr}	7.73	80.80	2947.70
SpeechVAE w/ $\mathcal{L}_{p,\log MSE}$, \mathcal{L}_{rr}	6.20	59.78	1530.81
SpeechVAE w/ $\mathcal{L}_{p,\log MSE}$, \mathcal{L}_{rr} , dim=256	6.28	65.63	1757.95

can be quantified and analyzed qualitatively by listening and comparing the original and reconstructed audio samples. PCA attains the highest reconstruction accuracy but has poor smoothness properties and does not strike along the other dimensions. Interpretability in the disentangled space (lower half of Table 1) has a relatively low toll on the SNR, a reduction from 4.43 to 4.16. MNIST proved less stable to train and does not fair well with the cycle loss, perhaps due to having a lower dimensionality compared to the audio encoding.

We further analyze the effect of the additional constraints on the audio autoencoder by measuring its throughput individually. Out of the models with smoothness, $\mathcal{L}_{p,\log MSE}$ with $\lambda_p = 10^3$ attains the highest reconstruction quality (SNR) and lowest latent space velocity calculated with finite differences. The disentanglement reduces audio reconstruction significantly. However, this has limited effect on the overall throughput, as analyzed before, likely due to bottlenecks in the visual model dominating the overall accuracy.

4.3. Temporal Smoothness Effectiveness

Mapping from audio to video with VAEs without constraints and PCA leads to choppy results, with mean latent space velocities above $300 s^{-1}$. We visualize the gain in smoothness in Figure 9 by plotting the high-dimensional latent trajectory embedded into three dimensions using multi-dimensional scaling (MDS) [8]. The gain is similar for all of the proposed smoothness constraints. The supplemental videos show how the smoothness eases information perception.

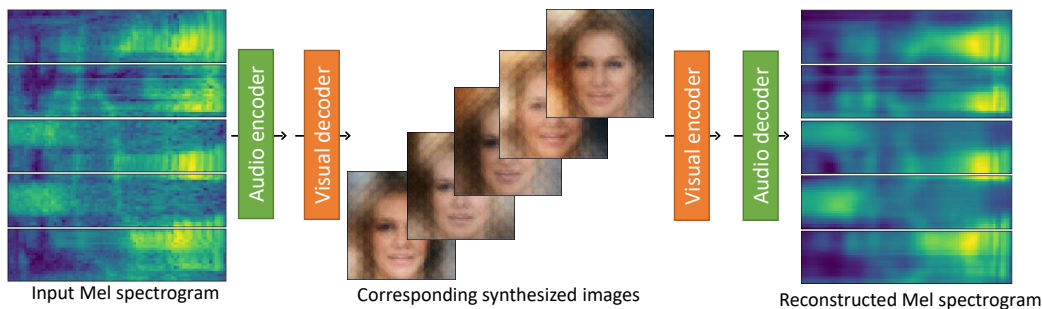


Figure 8. **Throughput.** The information throughput can be measured by mapping from audio to video and back. Playing the depicted Mel Spectrogram shows that the speech is still recognizable.

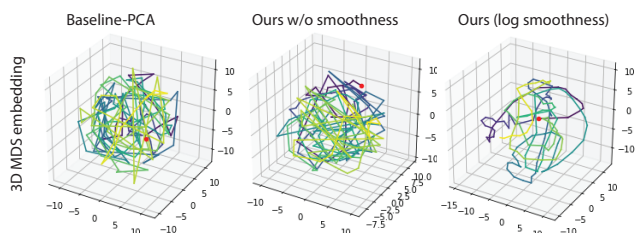


Figure 9. **Smoothness evaluation** by plotting the latent embedding of an audio snippet in 3D via dimensionality reduction. **Left:** Without smoothness constraint, consecutive audio sample embeddings are scattered. **Right:** Our full model leads to smoother trajectories.

4.4. Visual Domain Influence

Earlier work [5, 25] suggests that faces are suitable for representing high-dimensional data. Our experiments support this finding in that the measurable information content is larger. The SNR of the jointly trained CelebA models is larger than the MNIST models. Also the Figure 7 indicates that facial models are richer. The distinctiveness is further analyzed in the user study evaluation.

4.5. User study

We analyze the gain from a disentangled latent space vs. a combined one and the difference of using faces or digits for visualization with a user study among 19 participants answering 29 questions, with the same question repeated for the three visualization techniques mentioned above and with questions randomized.

Identifying and distinguishing sounds. Our user study analyzes the ability to distinguish between visualizations of different sounds, similar to the ones show in Figure 7 and the results are show in Table 3. Overall, the users were able to correctly recognize visualizations for the same sound with an accuracy of 85.4% for the CelebA content model and 79.7% for the MNIST content model. Broken down by tasks, users for the CelebA model achieve the better accuracy of 84.6%

Table 3. **User study results.** User answer accuracy in percent (\pm std.) for distinguishing between visualizations of different sounds, broken down by question type and phone-pairs vs words.

	CelebA	MNIST
Matching questions	84.5 \pm 13.8	77.4 \pm 10.6
Grouping questions	85.2 \pm 8.8	80.8 \pm 8.4
Phone-pairs	85.7 \pm 11.2	91.8 \pm 9.2
Words	84.5 \pm 8.6	73.8 \pm 7.3
Overall	85.0 \pm 6.8	79.7 \pm 6.5

in correctly matching one of two visualizations against a reference (random guessing yields 50%), while for the task of grouping four visualizations into pairs, users achieved an accuracy of 85.8 % (random guessing yields 33.3%).

Latent space disentanglement. Visualizing the style and content part separately with our full model significantly improves recognition scores. The disentangled face model increases the accuracy for distinguishing between speakers of different sex from 41.5 \pm 9.0% to 77.1 \pm 10.7% and speakers of different dialects from 15.4 \pm 16.3% to 57.1 \pm 22.8%. An AudioViewer prototype should therefore use the full model and show separate visual decodings side by side or have the option to switch between content and style visualization.

The user study is reported in full in the supplemental document.

5. Limitations and Future Work

Users were sometimes confusing the visualization of sounds and words and not all dialects could be distinguished. This may improve with users learning the specifics of the method but could also be further supported by making the method more intuitive and provide higher information content with more powerful face generators. In the future, we plan to integrate realistic lip motion for spoken sounds that are captured in the lip motion while maintaining the proposed general encoding for those that are not for environment sounds. Environment sounds lose higher frequencies

since trained on speech.

6. Conclusion

We presented AudioViewer, a new approach for visualizing audio via generative models coupled with cycle consistency and smoothness constraints. We have explored different generative models and target domains and found that while visualizations based on CelebA faces have richer features and a higher SNR, the visualizations based on the MNIST digits translated with VAEs give the most consistent mapping that is best recognized by human participants as indicated per our user study. Because our method is self-supervised, personalized models for any languages or sound domain can be learned. We hope that our approach will catalyze the development of future tools for assisting with handicaps linked to perceiving subtle audio differences.

References

- [1] Aguirre, G.K., Zarahn, E., D’esposito, M.: An area within human ventral cortex sensitive to “building” stimuli: evidence and implications. *Neuron* **21**(2), 373–383 (1998) [2](#)
- [2] Briot, J.P., Hadjeres, G., Pachet, F.D.: Deep learning techniques for music generation—a survey. *arXiv preprint arXiv:1709.01620* (2017) [3](#)
- [3] Cappelletta, L., Harte, N.: Phoneme-to-viseme mapping for visual speech recognition. In: *ICPRAM* (2). pp. 322–329 (2012) [3](#)
- [4] Chen, L., Li, Z., K Maddox, R., Duan, Z., Xu, C.: Lip movements generation at a glance. In: *Proceedings of the European Conference on Computer Vision (ECCV)*. pp. 520–535 (2018) [3](#)
- [5] Chernoff, H.: The use of faces to represent points in k-dimensional space graphically. *Journal of the American statistical Association* **68**(342), 361–368 (1973) [2](#), [8](#)
- [6] Chu, C., Zhmoginov, A., Sandler, M.: CycleGAN, a master of steganography. *arXiv preprint arXiv:1712.02950* (2017) [3](#)
- [7] Chung, J.S., Jamaludin, A., Zisserman, A.: You said that? *arXiv preprint arXiv:1705.02966* (2017) [3](#)
- [8] Cox, M.A., Cox, T.F.: Multidimensional scaling. In: *Handbook of data visualization*, pp. 315–347. Springer (2008) [7](#)
- [9] Dong, H.W., Hsiao, W.Y., Yang, L.C., Yang, Y.H.: MuseGAN: Multi-track sequential generative adversarial networks for symbolic music generation and accompaniment. In: *Thirty-Second AAAI Conference on Artificial Intelligence* (2018) [3](#)
- [10] Duarte, A., Roldan, F., Tubau, M., Escur, J., Pascual, S., Salvador, A., Mohedano, E., McGuinness, K., Torres, J., Giro-i Nieto, X.: Wav2pix: speech-conditioned face generation using generative adversarial networks. In: *IEEE International Conference on Acoustics, Speech and Signal Processing (ICASSP)*. vol. 3 (2019) [2](#)
- [11] Eberhardt, S.P., Bernstein, L.E., Coulter, D.C., Hunckler, L.A.: Omar a haptic display for speech perception by deaf and deaf-blind individuals. In: *Proceedings of IEEE Virtual Reality Annual International Symposium*. pp. 195–201. IEEE (1993) [3](#)
- [12] Elssmann, S.F., Maki, J.E.: Speech spectrographic display: use of visual feedback by hearing-impaired adults during independent articulation practice. *American Annals of the Deaf* pp. 276–279 (1987) [1](#), [3](#)
- [13] Fernandez-Lopez, A., Sukno, F.M.: Optimizing phoneme-to-viseme mapping for continuous lip-reading in Spanish. In: *International Joint Conference on Computer Vision, Imaging and Computer Graphics*. pp. 305–328. Springer (2017) [3](#)
- [14] Garofolo, J.S.: Timit acoustic phonetic continuous speech corpus. Linguistic Data Consortium, 1993 (1993) [6](#)
- [15] Goldish, L.H., Taylor, H.E.: The optacon: A valuable device for blind persons. *Journal of Visual Impairment & Blindness* **68**(2), 49–56 (1974) [3](#)
- [16] Goodfellow, I., Pouget-Abadie, J., Mirza, M., Xu, B., Warde-Farley, D., Ozair, S., Courville, A., Bengio, Y.: Generative adversarial nets. In: *Advances in neural information processing systems*. pp. 2672–2680 (2014) [2](#)
- [17] Hao, W., Zhang, Z., Guan, H.: CmcGAN: A uniform framework for cross-modal visual-audio mutual generation. In: *Thirty-Second AAAI Conference on Artificial Intelligence* (2018) [3](#)
- [18] Hardcastle, W.J., Gibbon, F.E., Jones, W.: Visual display of tongue-palate contact: electropalatography in the assessment and remediation of speech disorders. *International Journal of Language & Communication Disorders* **26**(1), 41–74 (1991) [3](#)
- [19] Hiasa, Y., Otake, Y., Takao, M., Matsuoka, T., Takashima, K., Carass, A., Prince, J.L., Sugano, N., Sato, Y.: Cross-modality image synthesis from unpaired data using CycleGAN. In: *International workshop on simulation and synthesis in medical imaging*. pp. 31–41. Springer (2018) [3](#)

- [20] Hou, X., Shen, L., Sun, K., Qiu, G.: Deep feature consistent variational autoencoder. In: 2017 IEEE Winter Conference on Applications of Computer Vision (WACV). pp. 1133–1141 (2017) [2](#), [5](#)
- [21] Hsu, W.N., Zhang, Y., Glass, J.: Learning latent representations for speech generation and transformation. In: Interspeech. pp. 1273–1277 (2017) [3](#), [4](#), [7](#)
- [22] Hu, D., Wang, D., Li, X., Nie, F., Wang, Q.: Listen to the image. In: Proceedings of the IEEE/CVF Conference on Computer Vision and Pattern Recognition (CVPR) (June 2019) [3](#)
- [23] Huang, X., Belongie, S.: Arbitrary style transfer in real-time with adaptive instance normalization. In: Proceedings of the IEEE International Conference on Computer Vision. pp. 1501–1510 (2017) [3](#)
- [24] IBM: Speech viewer iii (2004) [3](#)
- [25] Jacob, R.J., Egeth, H.E.: The face as a data display. *Human Factors* **18**(2), 189–200 (1976) [2](#), [8](#)
- [26] Jha, A.H., Anand, S., Singh, M., Veeravasarapu, V.: Disentangling factors of variation with cycle-consistent variational auto-encoders. In: European Conference on Computer Vision. pp. 829–845. Springer (2018) [3](#), [5](#)
- [27] Kamper, H.: Truly unsupervised acoustic word embeddings using weak top-down constraints in encoder-decoder models. In: ICASSP 2019-2019 IEEE International Conference on Acoustics, Speech and Signal Processing (ICASSP). pp. 6535–3539. IEEE (2019) [3](#)
- [28] Kanwisher, N., Stanley, D., Harris, A.: The fusiform face area is selective for faces not animals. *Neuroreport* **10**(1), 183–187 (1999) [2](#)
- [29] Karras, T., Aila, T., Laine, S., Herva, A., Lehtinen, J.: Audio-driven facial animation by joint end-to-end learning of pose and emotion. *ACM Transactions on Graphics (TOG)* **36**(4), 1–12 (2017) [2](#)
- [30] Karras, T., Laine, S., Aila, T.: A style-based generator architecture for generative adversarial networks. In: Proceedings of the IEEE Conference on Computer Vision and Pattern Recognition. pp. 4401–4410 (2019) [3](#)
- [31] Katz, W.F., Mehta, S.: Visual feedback of tongue movement for novel speech sound learning. *Frontiers in human neuroscience* **9**, 612 (2015) [3](#)
- [32] Kingma, D.P., Welling, M.: Auto-encoding variational bayes. arXiv preprint arXiv:1312.6114 (2013) [2](#), [4](#)
- [33] Kröger, B.J., Birkholz, P., Hoffmann, R., Meng, H.: Audiovisual tools for phonetic and articulatory visualization in computer-aided pronunciation training. In: Development of multimodal interfaces: Active listening and synchrony, pp. 337–345. Springer (2010) [1](#), [3](#)
- [34] LeCun, Y., Bottou, L., Bengio, Y., Haffner, P.: Gradient-based learning applied to document recognition. *Proceedings of the IEEE* **86**(11), 2278–2324 (1998) [6](#)
- [35] Levis, J., Pickering, L.: Teaching intonation in discourse using speech visualization technology. *System* **32**(4), 505–524 (2004) [3](#)
- [36] Lidestam, B., Beskow, J.: Visual phonemic ambiguity and speechreading. *Journal of Speech, Language, and Hearing Research* (2006) [3](#)
- [37] Liu, Z., Luo, P., Wang, X., Tang, X.: Deep learning face attributes in the wild. In: Proceedings of International Conference on Computer Vision (ICCV) (December 2015) [6](#)
- [38] Maidenbaum, S., Abboud, S., Amedi, A.: Sensory substitution: Closing the gap between basic research and widespread practical visual rehabilitation. *Neuroscience & Biobehavioral Reviews* **41**, 3–15 (2014) [3](#)
- [39] Musk, E., et al.: An integrated brain-machine interface platform with thousands of channels. *Journal of medical Internet research* **21**(10), e16194 (2019) [1](#)
- [40] Newman, J.L., Theobald, B.J., Cox, S.J.: Limitations of visual speech recognition. In: Auditory-Visual Speech Processing 2010 (2010) [3](#)
- [41] Noda, K., Yamaguchi, Y., Nakadai, K., Okuno, H.G., Ogata, T.: Audio-visual speech recognition using deep learning. *Applied Intelligence* **42**(4), 722–737 (2015) [2](#)
- [42] Öster, A.: Teaching speech skills to deaf children by computer-based speech training. *STL-Quarterly Progress and Status Report* **36**(4), 67–75 (1995) [2](#), [3](#)
- [43] Park, S.H., Kim, D.J., Lee, J.H., Yoon, T.S.: Integrated speech training system for hearing impaired. *IEEE Transactions on Rehabilitation Engineering* **2**(4), 189–196 (1994) [3](#)
- [44] Piczak, K.J.: Esc: Dataset for environmental sound classification. In: Proceedings of the 23rd ACM international conference on Multimedia. pp. 1015–1018 (2015) [6](#)

- [45] Povey, D., Ghoshal, A., Boulianne, G., Burget, L., Glembek, O., Goel, N., Hannemann, M., Motlicek, P., Qian, Y., Schwarz, P., et al.: The kald speech recognition toolkit. In: IEEE 2011 workshop on automatic speech recognition and understanding. No. CONF, IEEE Signal Processing Society (2011) 6
- [46] Sadoughi, N., Busso, C.: Speech-driven expressive talking lips with conditional sequential generative adversarial networks. *IEEE Transactions on Affective Computing* (2019) 2
- [47] Shlizerman, E., Dery, L., Schoen, H., Kemelmacher-Shlizerman, I.: Audio to body dynamics. In: Proceedings of the IEEE Conference on Computer Vision and Pattern Recognition. pp. 7574–7583 (2018) 2
- [48] Sperling, G.: The information available in brief visual presentations. *Psychological monographs: General and applied* 74(11), 1 (1960) 2
- [49] Stewart L, L.W., R, H.: A real-time sound spectrograph with implications for speech training for the deaf. In: IEEE International Conference Acoustics Speech and Signal Processing (1976) 2, 3
- [50] Suwajanakorn, S., Seitz, S.M., Kemelmacher-Shlizerman, I.: Synthesizing obama: learning lip sync from audio. *ACM Transactions on Graphics (TOG)* 36(4), 1–13 (2017) 2
- [51] Taigman, Y., Polyak, A., Wolf, L.: Unsupervised cross-domain image generation. *arXiv preprint arXiv:1611.02200* (2016) 3
- [52] Takahashi, T., Fukayama, S., Goto, M.: Instrudiver: A music visualization system based on automatically recognized instrumentation. In: ISMIR. pp. 561–568 (2018) 3
- [53] Tarr, M.J., Gauthier, I.: Ffa: a flexible fusiform area for subordinate-level visual processing automatized by expertise. *Nature neuroscience* 3(8), 764–769 (2000) 2
- [54] Taylor, S., Kim, T., Yue, Y., Mahler, M., Krahe, J., Rodriguez, A.G., Hodgins, J., Matthews, I.: A deep learning approach for generalized speech animation. *ACM Transactions on Graphics (TOG)* 36(4), 1–11 (2017) 2
- [55] Tian, Y., Engel, J.: Latent translation: Crossing modalities by bridging generative models. *arXiv preprint arXiv:1902.08261* (2019) 3
- [56] Tmenova, O., Martin, R., Duong, L.: CycleGAN for style transfer in x-ray angiography. *International journal of computer assisted radiology and surgery* 14(10), 1785–1794 (2019) 3
- [57] Vougioukas, K., Petridis, S., Pantic, M.: End-to-end speech-driven facial animation with temporal GANs. *arXiv preprint arXiv:1805.09313* (2018) 3
- [58] Wen, Y., Singh, R., Raj, B.: Reconstructing faces from voices. *arXiv preprint arXiv:1905.10604* (2019) 2
- [59] Wiles, O., Sophia Koepke, A., Zisserman, A.: X2face: A network for controlling face generation using images, audio, and pose codes. In: Proceedings of the European Conference on Computer Vision (ECCV). pp. 670–686 (2018) 2
- [60] Xu, W., Lifang, X., Dan, Y., Zhiyan, H.: Speech visualization based on robust self-organizing map (rsom) for the hearing impaired. In: 2008 International Conference on BioMedical Engineering and Informatics. vol. 2, pp. 506–509. IEEE (2008) 1, 3
- [61] Yang, D., Xu, B., Wang, X.: Speech visualization based on improved spectrum for deaf children. In: 2010 Chinese Control and Decision Conference. pp. 4377–4380. IEEE (2010) 1, 3
- [62] Yook, D., Leem, S.G., Lee, K., Yoo, I.C.: Many-to-many voice conversion using cycle-consistent variational autoencoder with multiple decoders. In: Proc. Odyssey 2020 The Speaker and Language Recognition Workshop. pp. 215–221 (2020) 3, 5
- [63] Yoshii, K., Goto, M.: Music thumbnailer: Visualizing musical pieces in thumbnail images based on acoustic features. In: ISMIR. pp. 211–216 (2008) 3
- [64] Yuan, L., Chen, Y., Fu, S., Wu, A., Qu, H.: SpeechLens: A visual analytics approach for exploring speech strategies with textural and acoustic features. In: 2019 IEEE International Conference on Big Data and Smart Computing (BigComp). pp. 1–8. IEEE (2019) 3
- [65] Zaccagnini, C.M., Antia, S.D.: Effects of multisensory speech training and visual phonics on speech production of a hearing-impaired child. *Journal of Childhood Communication Disorders* 15(2), 3–8 (1993) 2, 3
- [66] Zhou, H., Liu, Y., Liu, Z., Luo, P., Wang, X.: Talking face generation by adversarially disentangled audio-visual representation. In: Proceedings of the AAAI Conference on Artificial Intelligence. vol. 33, pp. 9299–9306 (2019) 3
- [67] Zhu, J.Y., Park, T., Isola, P., Efros, A.A.: Unpaired image-to-image translation using cycle-consistent adversarial networks. In: Proceedings of the IEEE international conference on computer vision. pp. 2223–2232 (2017) 3

Supplemental Document

AudioViewer: Learning to visualize sounds

Yuchi Zhang
University of British Columbia
Vancouver, Canada
yuchi45@cs.ubc.ca

Willis Peng
University of British Columbia
Vancouver, Canada
willispcpeng@gmail.com

Bastian Wandt
Leibniz University Hannover
Hannover, Germany
wandt@tnt.uni-hannover.de

Helge Rhodin
University of British Columbia
Vancouver, Canada
rhodin@cs.ubc.ca

This document provides an additional analysis and details on the user study, supplementing the main document. We also prepared an additional supplemental HTML file ([link](#)) that contains audio and video snippets that can not be played in a conventional PDF. These give additional qualitative results for spoken sentences and environment sounds.

1. Results on Environment Sounds

With the style disentangling training of our AudioViewer method, the audio model is more specific to human speech than general sounds. In the following, we test the generalization capability of our method (trained on the speech TIMIT dataset [1]) on the ESC-50 environment sound dataset [3].

Table 1 shows the reconstruction accuracy when going via the audio and video VAEs (see Information Throughput section in the main document). The SNR for reconstructed Mel spectrum is generally lower than the speech dataset, which is expected since it was trained on the latter. The

Table 1. **Information throughput on environment sounds**, showing that the reconstruction error increases when evaluating on a test set that contains sounds vastly different from the training set (speech vs. environment sounds).

Audio models	Visual models	SNR(dB)
Audio PCA	Visual PCA	17.23
SpeechVAE	DFC-VAE on CelebA	1.03
	DFC-VAE on MNIST	2.22
	DFC-VAE on CelebA (refined w/ \mathcal{L}_{cycle})	2.83
	DFC-VAE on MNIST (refined w/ \mathcal{L}_{cycle})	0.76
SpeechVAE w/ $\mathcal{L}_{p,\log MSE}, \mathcal{L}_{rr}, \dim=256$	DFC-VAE on CelebA	0.46
	DFC-VAE on MNIST	0.46
	DFC-VAE on CelebA (refined w/ \mathcal{L}_{cycle})	1.26
	DFC-VAE on MNIST (refined w/ \mathcal{L}_{cycle})	1.68

analysis of the reconstruction ability of the audio VAE in isolation (without going through the video VAE) reported in Table 2 shows that a large fraction of this loss of accuracy stems from the learning of speech specific features of the audio VAE. Moreover, with a recombined reconstruction loss term on the human speech dataset, the model was fitted to speech features and tended to loss high pitch information. Still, according to the face visualization of the content encoding as we showed in the HTML file, our AudioViewer can generate consistent visualization to given environment sounds.

2. Additional ablation study on λ_c and λ_p

Due to the low SNR of the disentangled model, here we report the ablation experiments on λ_c and λ_p without the disentangled training to better illustrate the performance of the two loss terms.

Table 2. **Audio VAE Mel spectrum reconstruction**. The average SNR of autoencoding and decoding Mel spectrograms on ESC-50 shows a significant reconstruction loss. The average speed and acceleration between the latent vector ($\dim = 128$) of neighbouring frames ($\Delta t = 0.04s$) confirms the experiments in the main document, that smoothness comes at the cost of lower reconstruction accuracy.

Audio models	SNR (dB)	Velocity (s^{-1})	Acc. (s^{-2})
Audio PCA	17.23	170.13	6960.80
SpeechVAE[2]	10.17	172.57	7331.77
SpeechVAE w/ $\mathcal{L}_{p,\log MSE}$	8.92	58.78	1859.95
SpeechVAE w/ \mathcal{L}_{rr}	2.98	40.54	1580.86
SpeechVAE w/ $\mathcal{L}_{p,\log MSE}, \mathcal{L}_{rr}$	2.19	30.66	909.39
SpeechVAE w/ $\mathcal{L}_{p,\log MSE}, \mathcal{L}_{rr}, \dim=256$	2.51	33.88	1037.97

Table 3 shows the reconstruction error on TIMIT, when reconstructing the Mel spectrum via the audio and video VAEs (see Information Throughput section in the main document). We compare versions where the visual VAEs are trained independently or refined with the audio ones using different weights λ_c for the cycle loss. Irrespective of the visual domain (CelebA or MNIST), $\lambda_c = 10$ works best together with the both temporal losses and is selected for the disentangled version. Moreover, as we have expected, the higher cycled reconstruction SNR indicates a higher capacity of information of face visualization than the figure ones.

Table 4 shows the reconstruction SNR (encoding followed by decoding with the audio VAE) on the test set with models trained with different loss functions, as in the main document but with a larger number of tested weights λ_p . The SpeechVAE w/ $\mathcal{L}_{p, \log MSE}$ with $\lambda_p = 10^3$ is the best performing model that was selected for disentangled model.

3. User Study

Our user study required participants to complete one of 4 versions of a questionnaire: disentangled content model with CelebA visualizations (CelebA-content), disentangled style

Table 3. **Experiments with different cycle loss weight λ_c .** Average SNR of cycle-reconstructed amplitude Mel spectrogram on the TIMIT test set.

Audio models	Visual models	λ_c	SNR(dB)
SpeechVAE w/ $\mathcal{L}_{p, \log MSE}$ ($\lambda_p = 10^3$)	DFC-VAE on CelebA	-	1.51
	DFC-VAE on MNIST	-	2.16
	DFC-VAE on CelebA (refined w/ L_c)	1	4.86
	DFC-VAE on MNIST (refined w/ L_c)	1	4.54
	DFC-VAE on CelebA (refined w/ L_c)	10	11.81
	DFC-VAE on MNIST (refined w/ L_c)	10	3.98
	DFC-VAE on CelebA (refined w/ L_c)	100	10.51
SpeechVAE w/ $\mathcal{L}_{p, Q}$ ($\lambda_p = 10^3$)	DFC-VAE on MNIST (refined w/ L_c)	100	5.22
	DFC-VAE on CelebA	-	1.96
	DFC-VAE on MNIST	-	1.87
	DFC-VAE on CelebA (refined w/ L_c)	1	5.95
	DFC-VAE on MNIST (refined w/ L_c)	1	7.06
	DFC-VAE on CelebA (refined w/ L_c)	10	12.25
	DFC-VAE on MNIST (refined w/ L_c)	10	3.12
SpeechVAE w/ $\mathcal{L}_{p, MSE}$	DFC-VAE on CelebA (refined w/ L_c)	100	8.71
	DFC-VAE on MNIST (refined w/ L_c)	100	5.26

Table 4. **Additional ablation study on λ_p .** The average SNR of reconstructed amplitude Mel spectrogram on the TIMIT test set and the average speed and acceleration between the latent vector (dim = 128) of neighbouring frames ($\Delta t = 0.04s$).

Audio models	λ_p	SNR (dB)	Velocity (s^{-1})	Acceleration (s^{-2})
Audio PCA	-	23.37	329.02	13395.11
SpeechVAE w/o \mathcal{L}_p	-	21.90	280.09	11648.17
SpeechVAE w/ $\mathcal{L}_{p, \log MSE}$	1	16.74	231.91	9490.04
	10^3	19.86	108.89	3052.19
	10^7	11.43	117.43	2674.86
	10^9	7.77	76.50	1735.97
	1	18.83	234.19	9595.15
SpeechVAE w/ $\mathcal{L}_{p, Q}$	10^3	18.44	119.94	3133.26
	10^7	11.35	123.78	2476.44
	10^9	9.00	119.60	2405.18
	1	17.89	243.55	10067.36
	SpeechVAE w/ $\mathcal{L}_{p, MSE}$	10^3	18.15	226.74
10^7		12.64	129.10	4192.21
10^9		10.56	84.05	2709.96

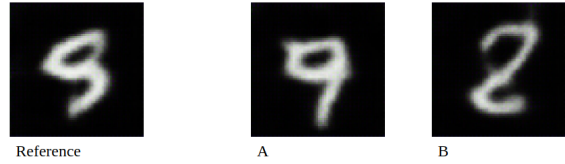
Question 11



Indicate the above image (A or B) that is most similar to the reference image:

A B

Question 11



Indicate the above image (A or B) that is most similar to the reference image:

A B

Figure 1. **Matching Example.** Examples from the CelebA-combined and MNIST-content questionnaire of a matching question asked to participants in the user study.

model with CelebA visualizations (CelebA-style), disentangled content model with MNIST visualizations (MNIST-content) and a combined model with CelebA visualizations (CelebA-combined). Each version of the questionnaire asked the same set of 29 questions with randomized ordering of answers within each question. The study was conducted with 14, 15, 12, and 14 participants for the CelebA-content, CelebA-style, CelebA-combined and MNIST-content questionnaires, respectively. Amongst all the questionnaires, there were 27 unique participants. It took participants between 10-15 minutes to complete the each questionnaire. In addition, the questionnaire did not indicate the purpose of the underlying research and only asked participant to perform two possible tasks: matching and grouping visualizations. The format of the questionnaire is outlined in Table 5. The questions tested for two factors: sound content, sounds that share the same phoneme sequences, and sound style, sounds produced by speakers of the same sex or speaker dialect. This purely visual comparison allows us analyze different aspects individually.

Matching questions Matching questions asked the participants to choose which of two possible visualizations which is most visually similar to a given reference visual. Figure 1 shows examples of matching questions. Matching questions were used to assess the viability for users to distinguish between the same sounds produced by speakers

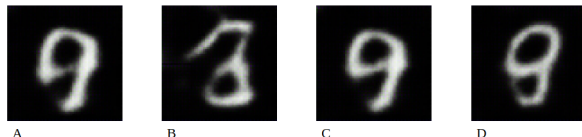
Question 23



Group the above images (A - D) into pairs of similar images:

- AB, CD AC, BD AD, BC

Question 23



Group the above images (A - D) into pairs of similar images:

- AB, CD AC, BD AD, BC

Figure 2. **Grouping Example.** Examples from the CelebA-combined and MNIST-content questionnaire of a grouping question asked to participants in the user study.

Table 5. **A breakdown of the questionnaire format** by sound type and tested factors, listing their frequency of occurrence.

Question type	Sound type	Tested factor	Questions
Matching questions	Phone-pairs	Content	3
		Style (sex)	3
		Style (dialect)	2
	Words	Content	3
		Style (sex)	3
		Style (dialect)	2
Grouping questions	Phone-pairs	Content + style (dialect)	2
		Content + style (dialect + sex)	2
	Words	Content	3
		Content + style (dialect)	2
		Content + style (sex)	1
		Content + style (dialect + sex)	1
		Content (similar sounding words)	2
Total			29

possessing different speaker traits as well as determining whether structural similarities in the underlying audio translated into similarities in the visualization. In particular, the questionnaire contained 6 questions for evaluating the ability to distinguish between sound content, which compared visualizations of sounds of different phoneme sequences (3 for phoneme-pairs and 3 for words). Phone-pairs are short in length and therefore the corresponding visualisation was a single frame image, whereas visualisations of words were videos. In order to evaluate the ability to distinguish between sound style, 6 questions compared visualizations of the same phoneme sequence between male and female speakers and 4 questions for distinguishing between speakers of different dialects. In total there were 16 matching questions. Since each question has two options, the expected mean accuracy

Table 6. **User study results.** Values indicate mean accuracy and standard deviation for distinguishing between visualizations of the tested factor across participants as a percentage.

Tested Factor	Sub-type	Baseline	CelebA-disentangled	CelebA-combined	MNIST-content
Content	Phone-pairs	40.3	85.7 ± 11.2	70.2 ± 9.6	91.8 ± 9.2
	Words	37.3	84.5 ± 8.6	74.3 ± 14.0	73.8 ± 7.2
	Matching	50.0	84.5 ± 13.8	84.7 ± 4.8	77.4 ± 10.6
	Grouping	33.3	85.2 ± 8.8	67.3 ± 14.0	80.8 ± 8.4
	Overall	38.4	85.0 ± 6.8	72.8 ± 10.0	79.7 ± 6.5
Style (dialect)	Overall	50.0	56.7 ± 22.1	39.6 ± 24.9	-
Style (sex)	Overall	43.3	78.0 ± 10.8	43.3 ± 8.9	-

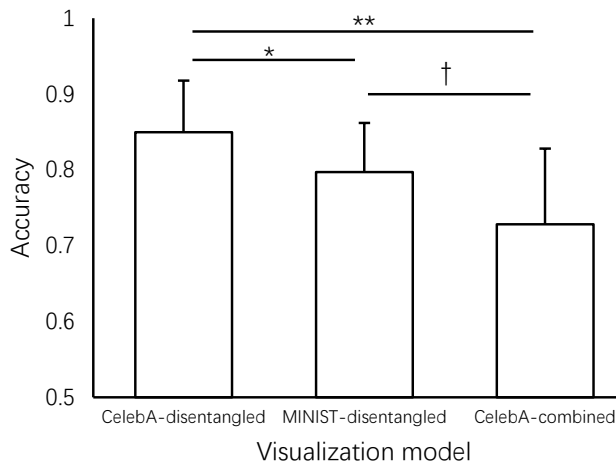


Figure 3. **Model Comparison on content questions.** The mean user accuracy and standard deviation for distinguishing phoneme sequences is compared between the models, annotated with the significance level († for $0.05 < p < 0.1$, * for $p < 0.05$, ** for $p < 0.01$). The mean accuracy for random guessing is 0.384.

for random guessing is 50%.

Grouping questions Grouping questions asked the participants to group 4 visualizations into two pairs of similar visualizations. Figure 2 shows examples of grouping questions. Grouping questions were used to assess the degree to which visualizations of different words are distinguishable and visualizations of the same word are similar. In particular, the study required users to group visualizations of two pairs of sounds, whereby different pairs are sound clips with shared factors of the same sound content or same sound style. In total, the user study consisted of 4 grouping questions based on phone-pairs and 9 grouping questions based on words. Since there are three possible options, the expected mean accuracy for random guessing is 33.3%.

3.1. Results

For each of the three models, we tested for sound content: phoneme sequences, and sound style: speaker dialect and speaker sound. We generated the mean accuracy and standard deviation for each tested factor and each question sub-type as shown in Table 6. The results of the disentangled models with CelebA visualizations (CelebA-disentangled)

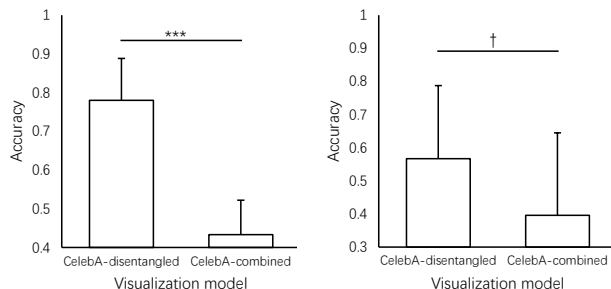


Figure 4. **Model Comparison on style questions.** The mean user accuracy and standard deviation for distinguishing speaker sex (left) and dialect(right) is compared between the models, annotated with the significance level († for $0.05 < p < 0.1$, *** for $p < 0.001$). The mean accuracies for random guessing are 0.43 and 0.5 respectively.

is aggregated by taking the results of CelebA-content on the questions which tested for sound content and the results of CelebA-style on questions which tested for sound style. Since we only evaluated the disentangled content model for the MNIST visualizations, it is only compared for the content questions. Significance comparing model means were calculated using a two-sample two-tailed t-test with unequal variance and without any outlier rejection.

Figure 3 shows users achieve the highest overall accuracy on the CelebA-disentangled model with $85.0 \pm 6.8\%$ (significant with $p < 0.05$) for distinguishing between visualizations of different content. The MNIST-content model has the highest accuracy for distinguishing between different phone pairs with $91.8 \pm 9.2\%$, although not significantly higher than the CelebA-disentangled one with ($p > 0.05$), but has a much lower accuracy for distinguishing between different words, suggesting that the MNIST visualizations may be better suited for representing shorter sounds. The CelebA-disentangled model outperforms the CelebA-combined model for distinguishing between speakers of different sex with $78.0 \pm 10.8\%$ (significant with $p < 0.001$) and between speakers of different dialects with $56.7 \pm 22.1\%$ (marginally significant with $0.05 < p < 0.10$) as shown in Figure 4. The task of distinguishing between different speakers of different dialects is much more difficult than distinguishing between phoneme sequences since there are 8 categories of dialects in the dataset and differences in dialects are much more subtle and can often contain overlaps. This translates to lower accuracy in this question category.

References

[1] Garofolo, J.S.: Timit acoustic phonetic continuous speech corpus. Linguistic Data Consortium, 1993 (1993)

1

[2] Hsu, W.N., Zhang, Y., Glass, J.: Learning latent representations for speech generation and transformation. In: Interspeech. pp. 1273–1277 (2017) 1

[3] Piczak, K.J.: Esc: Dataset for environmental sound classification. In: Proceedings of the 23rd ACM international conference on Multimedia. pp. 1015–1018 (2015)

1